creative commons
COMMONS DEED

저작자표시-비영리-변경금지 2.0 대한민국

이용자는 아래의 조건을 따르는 경우에 한하여 자유롭게

- 이 저작물을 복제, 배포, 전송, 전시, 공연 및 방송할 수 있습니다.

다음과 같은 조건을 따라야 합니다:

저작자표시. 귀하는 원저작자를 표시하여야 합니다.

비영리. 귀하는 이 저작물을 영리 목적으로 이용할 수 없습니다.

변경금지. 귀하는 이 저작물을 개작, 변형 또는 가공할 수 없습니다.

- 귀하는, 이 저작물의 재이용이나 배포의 경우, 이 저작물에 적용된 이용허락조건을 명확하게 나타내어야 합니다.
- 저작권자로부터 별도의 허가를 받으면 이러한 조건들은 적용되지 않습니다.

저작권법에 따른 이용자의 권리는 위의 내용에 의하여 영향을 받지 않습니다.

이것은 이용허락규약(Legal Code)을 이해하기 쉽게 요약한 것입니다.

Disclaimer

dCollection

공학석사 학위논문

Roles of Zr and Pr in sulfur poisoned Pd/Ce-based catalyst for CO oxidation

일산화탄소 산화반응에서 황 피독된 Pd/Ce계 촉매에서의 Zr와 Pr의 역할

2014년 6월

서울대학교 대학원

화학생물공학부

유영석

Abstract

Roles of Zr and Pr in sulfur poisoned Pd/Ce-based catalyst for CO oxidation

Youngseok Ryou

Master's Program

School of Chemical and Biological Engineering

Seoul National University

The diesel engines have drawn interest mainly due to their economic advantages arising from the superior fuel economy. While the regulations on diesel engine emission become more stringent, various catalytic systems are required to effectively remove environmentally harmful gases such as CO, hydrocarbon (HC), soot and NOx. Diesel oxidation catalyst (DOC) plays a key role in converting CO and unburned HCs to CO_2 and H_2O. DOC system requires low ignition temperature, hydrothermal stability and sulfur resistance. CeO_2 is essential support material in DOC for lower light-off temperature because of its excellent oxygen storage capacity (OSC). However, it is easily deactivated by high temperature treatment and sulfur poisoning. In this study,

CeZr and CeZrPr mixed-oxide solid solutions are used as catalyst support in comparison with pure CeO_2 to overcome these drawbacks

Pd 2wt% was loaded by incipient wetness impregnation. After impregnation, the catalysts were calcined at 500 ℃ and then, hydrothermally treated at 750 ℃. Those samples were designated as “Fresh” and “HTA”, respectively. In sulfur aging process, the HTA samples were treated with SO_2 containing gases. After that, regeneration process was followed. The sulfur aging and regenerated samples were named as “SA” and “DeSOx”, respectively.

To get information of the physicochemical properties of catalysts, various analyses were carried out by the means of XRD, BET, FT-IR, Elemental analysis, CO-chemisorption, H_2-TPR and SO_2-TPD experiment. Also, CO oxidation experiments were performed for these differently treated catalysts.

Fresh Pd/CeO_2 sample exhibits the highest CO oxidation ability because of high dispersion and surface area. After HTA treatment, H_2-TPR results indicate the enhancement of the interaction between Pd and support, which results in the improved catalytic activity in all samples. As evidenced by FT-IR, the sulfation treatment on Pd/CeO_2 induced the formation of $Ce(SO_4)_2$, which causes blocking the Pd active site and the decrease in surface area. In addition, it gives rise to the interruption of oxygen back-spillover from CeO_2 to Pd surface as a result of the weak interaction between Pd and CeO_2. Consequently, the activity in the low temperature region disappears. Among the SA samples, Pd/CeZrPr shows superior catalytic activity, because Pr complements the interaction between Pd and support through OSC property. After regeneration process, the Pd/CeZr recovers CO oxidation ability most significantly among the

samples. The XRD and BET results demonstrate that Pd/CeZr has outstanding sulfur resistance. In case of Pd/CeO_2, sulfur adsorption and desorption lead to structural collapse, which causes sintering and reduction of surface area. Therefore, the catalytic activity of Pd/CeO_2 is worse than that of sulfated sample.

This study reveals the promotional effect of Zr and Pr on Pd/CeO_2 catalyst during the sulfur adsorption/desorption process. Pr plays a role in minimizing the decrease in activity during the sulfur aging. The addition of Zr in CeO_2 disturbs sulfur adsorption and aids in maintaining the textural property and removing sulfur during DeSOx, thus leading to recover the activity considerably.

Keywords: CO oxidation, palladium catalyst, cerium oxide, zirconium,

Praseodymium, sulfur

Student Number: 2012-23269

Contents

List of Tables

List of Figures

Chapter 1. Introduction

1.1. Background of diesel oxidation catalyst

In modern automotive industry, diesel engines have attracted attention mainly due to their strengths on fuel efficiency, economy, power ability and durability [1-5]. However diesel engine emits various hazardous gases and substance such as carbon monoxide (CO), hydrocarbons (HCs), nitrogen oxides (NOx), volatile organic compounds (VOCs) and particulate matter (PM) to the atmosphere [6-8]. The diesel engine emissions are one of the cause of environmental pollution and human diseases [9-14]. In order to reduce pollutant, engine exhaust regulations are continuously being tighten in the world [15-18]. The European standard Euro VI for heavy-duty vehicles came into force in January 2013 [19]. And for light-duty vehicles will enforce in September 2014 [20]. There are two way for reducing harmful exhaust emission in diesel engine: enhancing the engine conversion efficiency or improving after-treatment systems. The after-treatment system using catalytic converter is one of the most effective method to reduce pollutants in exhaust gases. For example, three-way catalyst oxidizes CO, HCs and reduces NOx simultaneously with specific air-to-fuel ratio (14.5) in the gasoline engine [21-24]. However, the diesel engine has inefficient behavior with three-way catalyst. Reduction of NOx is interrupted by the excess oxygen environment of diesel engine [6, 8, 25]. In

order to decrease harmful component of diesel exhaust, multiple strategies are required. The typical after-treatment systems for diesel vehicles are made up of diesel oxidation catalyst (DOC), Diesel particulate filter (DPF), NOx selective reduction catalyst (SCR) and Lean NOx trap (LNT) [6, 8, 26]. Among them, DOC plays an important role with three major functions in a diesel exhaust control system. First of all, DOC oxidizes CO and unburned HCs to CO_2 and H_2O in emission [9, 27-29], and converts excess amount of fuel offered by post-injection to produce the essential heat for the regeneration of DPF [30]. Furthermore, DOC oxidizes NO to NO_2 and supports low temperature SCR performance [15]. The platinum group metal (PGM) is commonly used as active site component for reaction. Supported Pt catalysts are mostly applied as DOC because of their high oxidation performance [31]. However, Pt is readily deactivated in a high temperature condition [6, 32]. Although, Pd, another PGM, has more thermal durability, also has lower oxidation ability than Pt [33-35]. To improve physicochemical properties of Pt and Pd, Pt-Pd bimetallic catalysts have been researched [25, 32]. Support material is important for increasing catalytic activity. Al_2O_3 [24, 25, 33] and SiO_2 [25, 36] are normally employed as a support because of its high surface area and stability.

1.2. Objective

DOC requires some properties for its purpose. Since the location of the DOC is next to the engine, it tends to deteriorate under hydrothermal environment in the form of PGM sintering and the surface area disruption. In addition, the sulfur in commercial fuel leads to the gradual deactivation of catalytic performance. The cerium (IV) oxide (CeO_2) is an important component to lower ignition temperature in DOC because of its excellent oxygen storage capacity (OSC) [37-39]. However, it is readily damaged by high temperature and sulfur poisoning [39-41]. The insertion of ZrO_2 into a CeO_2 results in a mixed oxide solid solution [42]. This improves the physicochemical properties, such as thermal stability and redox ability by producing an efficient Ce^{4+}/Ce^{3+} redox cycle [39, 40, 42]. Also Pr can be used as an OSC component [43]. However, this substance was not much investigated for the DOC. This research aims at comprehending the role of Zr and Pr in sulfur-poisoned and regenerated Pd/CeO2, Pd/CeZr, Pd/CeZrPr catalysts for CO oxidation.

Chapter 2. Experimental

2.1. Catalyst preparation

Three commercial materials (CeO_2, $Ce_{0.7}Zr_{0.3,}$ $Ce_{0.65}Zr_{0.27}Pr_{0.8}$) were used as a support. Pd 2wt% catalyst were prepared by conventional incipient wetness impregnation (IWI) method with aqueous Pd $(NO_3)_2 \cdot 2H_2O$ (Sigma Aldrich) solution at ambient temperature. After impregnation, the catalysts were dried at 100 ℃ oven for 24h, and calcined at 500 ℃ in 15% O_2 with N_2 balance for 2h. Those catalysts were denoted as "Fresh". The "Fresh" catalysts were aged at 750 ℃ with distilled water for 25h. Those hydrothermally treated sample were abbreviated as "HTA (hydrothermal aging)"

In sulfur aging process, the HTA samples were aged by SO_2 containing gases (SO_2, H_2O, O_2 and N_2 in balance) at 300 ℃ for 24h. The sulfur treated samples were designated as "SA (sulfur aging)". After sulfur poisoning, regeneration process followed. To desorb SO_2, the SA samples were heated from room temperature to 750 ℃ under excess O_2 gas condition. The regenerated samples were named as "DeSOx".

2.2. Characterizations

2.2.1. XRD

The powder X-ray diffraction (XRD) patterns were recorded using a Rigaku (mode 1 smartlab) diffractometer with Cu Kα radiation (λ=0.1542 nm). The measurement voltage and current were 40 kV, 50 mA respectively. The scanning step size was 0.02 at a speed of 0.3. The patterns were collected in a 2 θ range from 10 to 80 °.

2.2.2. BET

Nitrogen adsorption-desorption isotherms were analyzed on a Micromeritics ASAP 2010 at liquid nitrogen temperature (-196 ℃). Prior to the analysis, all samples were degassed at 250 ℃ for 4h in evacuation condition. The specific surface area and pore size distribution were measured using the Brunauer-Emmett-Teller (BET) and Barrett-Joyner-Halenda (BJH) methods, respectively.

2.2.3. FT-IR

FT-IR spectra was collected on a M2000 (MIDAC Corp.) equipped with a pellet supporting device to get information of the sulfur amount and species.

The sample blended with KBr was pressed into pelletizer. The sample and KBr were mixed with the ratio of 1:49. All of the FT-IR experiments were carried out under vacuum at room temperature with a resolution of 4 cm^{-1} and 64 scans, with pure KBr background.

2.2.4. Elemental analysis

For the analysis of sulfur poisoning amount of catalyst, elemental analysis was performed on Leco Corp. (CHNS-932, Truspec 4640). The measurement was done several times for each catalyst. 1~2 mg of catalyst was used for each analysis.

2.2.5. CO-Chemisorption

In order to analyze dispersion and particle size of catalysts, CO-chemisorption was measured on a Micromeritics ASAP 2010. The 0.2g of each catalyst were pretreated by H_2 gas at 350 ℃ for 2h. After cooling down, CO-chemisorption was performed at room temperature.

2.2.6. H_2-TPR

H_2-temperature programmed reduction (H_2-TPR) was carried out to

investigate the reducibility of the catalysts in a BEL-CAT-BASIC (BEL Japan Inc.) with a thermal conductivity detector (TCD). All samples were pretreated in a flow of 15% O_2/N_2 at 500 ℃ for 2h at a rate of 100 cm^3min^{-1}. After cooling down, catalysts were exposed to 5% H_2/Ar mixed gas from room temperature to 750 ℃ at the rate of 10 ℃ /min.

2.3. Catalytic activity & SO_2-TPD (DeSOx)

The catalytic activity measurement was performed in a fixed-bed quartz tubular reactor. The 0.05 g of catalyst was diluted with 1.25 g of α-Al_2O_3 bead to distribute the additional heat produced during the reaction. The feed gas containing CO (1000 ppm), NO (100 ppm), H_2O, CO_2, O_2 and N_2 (balance) was introduced into the reactor using mass flow controllers. The mixture gas total flow rate and space velocity (SV) were 200 ml/min, 240,000 h^{-1} respectively. The reaction temperature was recorded by a K-type thermocouple placed on the top of the catalyst. The CO concentration of the outlet gas was measured by ULTRAMAT 23 gas analyzer (SIEMENS) during CO oxidation. When the reactor temperature reached 80 ℃, the preheated H_2O (at 120 ℃) was introduced to the reactor using syringe pump, then the reactor was heated from 80 to 400 ℃ at a rate of 2 ℃/min. The evolution of SO_2 during the DeSOx treatment was measured with the same except that heating range was from 80 to 750 ℃ with ramping rate of 10 ℃/min. In addition, the feed gas without CO

and NO is introduced for DeSOx treatment.

Chapter 3. Result & Discussion

3.1. XRD

The XRD patterns of various pretreated catalysts are included in Fig. 1-4. All catalysts clearly show fluorite cubic structure of CeO_2 [42, 44, 45]. The pure CeO_2 sample displays the reflections typical of the fluorite atomic structure with the (111), (200), (220) and (311) planes, corresponding to 28.5 °, 33.1 °, 47.6 ° and 56.4 ° [44, 46, 47]. No Pd phase peak is presented on the all XRD patterns, indicating that Pd particles are too small to be identified. The crystalline size using Scherrer equation [48] is shown in Table 1. For the Fresh catalysts, Pr contributes to the form of larger crystalline size (8.9 nm) than others. However, after hydrothermal aging, the average crystalline size is about 11.5 nm and 9.5 nm for CeO_2 and mixed-oxide catalyst respectively. After sulfur desorption process, different phenomenon is observed for pure CeO_2 and mixed-oxide catalysts. For the pure CeO_2 catalyst, the regeneration process leads to an increase in peak intensity and a decrease in width. In addition, the crystalline size increases to 26.5 nm. However, only the reduction of the peak intensity can be seen in the mixed-oxide catalysts. Those XRD results indicate that the mixed-oxides have stronger sulfur resistance than the pure ceria [40]. In Fig. 4, the diffractogram peaks of mixed-oxide samples are shifted to higher 2 θ compared to CeO_2 sample. The replacement of Ce^{4+} (0.097 nm) by Zr^{4+} (0.084 nm) causes shrinkage of lattice and reduces crystalline size. This

structural property makes peak shift and improves thermal stability of catalyst [42, 45].

3.2. BET & BJH method

The specific surface areas are given in Table 2. The CeO_2 has the highest surface area (86 m^2/g) for HTA sample. However, after sulfur aging process, all samples have similar surface area (38~40 m^2/g), representing that the CeO_2 is more contaminated by sulfur than other samples. The DeSOx samples show significantly different consequence for CeO_2 and mixed-oxides. In case of pure CeO_2, the surface area is reduced after DeSOx. On the other hand, the mixed-oxide catalysts recover its surface area. Although, it is not perfectly regenerated, mixed-oxide catalysts have more sulfur durability, in agreement with the XRD results. The pore size distributions calculated by BJH method are shown in Fig. 5-7. As can be seen, the pore diameter of mixed-oxide samples has similar range (10-30 nm) for the HTA, SA and DeSOx samples. On the contrary, The CeO_2 sample has higher pore diameter after various processes. Especially, after DeSOx treatment, the small diameter pores of CeO_2 vanished, demonstrating that structural collapse takes place on pure CeO_2 catalyst during the DeSOx process. Those results correspond with XRD result.

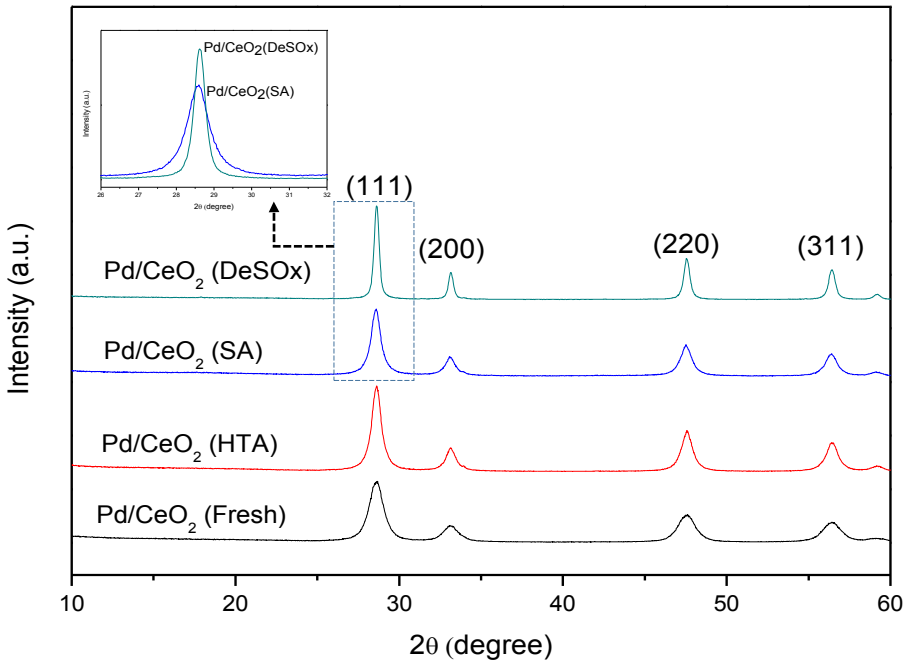

Fig. 1. XRD patterns of Pd/CeO_2 catalysts (Fresh, HTA, SA, DeSOx).

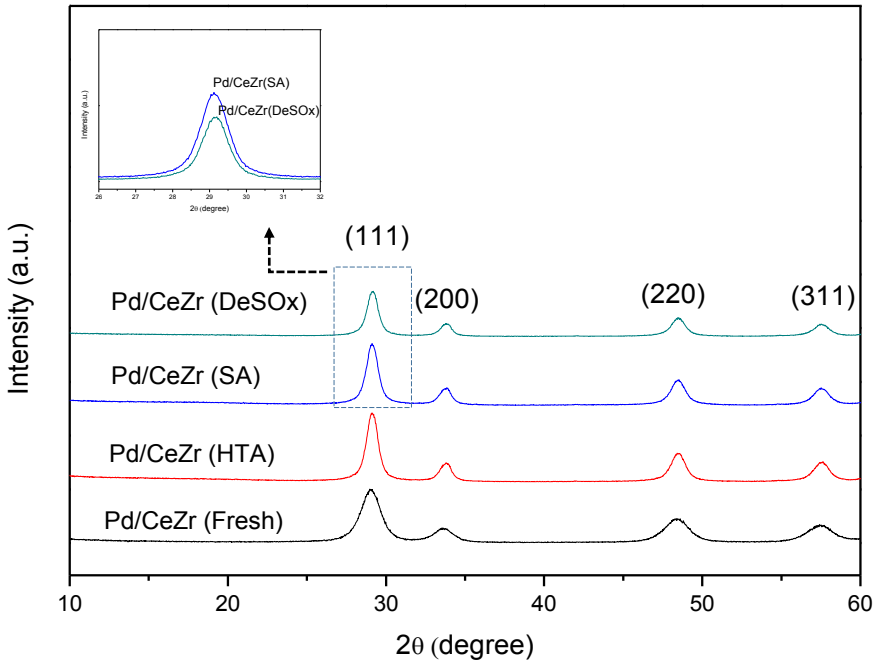

Fig. 2. XRD patterns of Pd/CeZr catalysts (Fresh, HTA, SA, DeSOx).

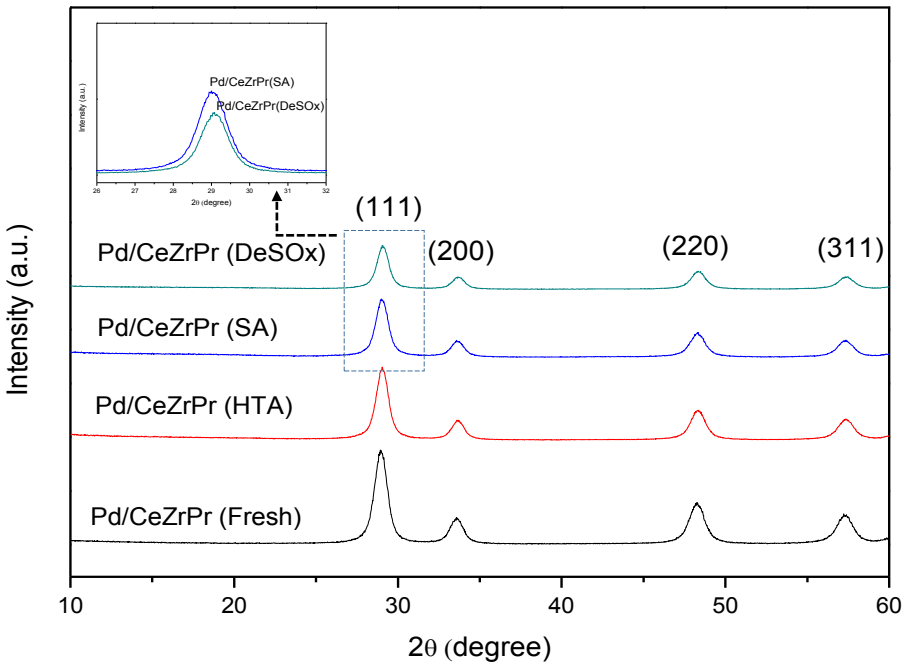

Fig. 3. XRD patterns of Pd/CeZrPr catalysts (Fresh, HTA, SA, DeSOx).

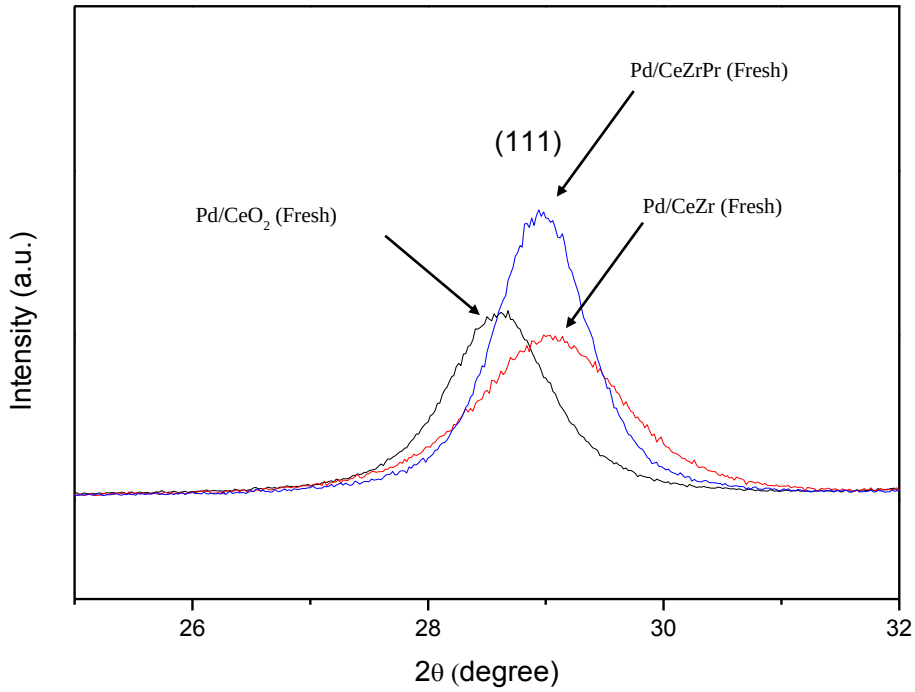

Fig. 4. XRD patterns of (111) plane for Fresh catalysts.

Table 1
Crystalline size of catalyst by Scherrer equation Unit : nm

Sample	Fresh	HTA	SA	DeSOx
Pd/CeO_2	7.9	11.5	11.5	26.5
Pd/CeZr	6.3	9.8	9.7	10.4
Pd/CeZrPr	8.9	9.5	9.5	10

Table 2
The specific surface area of catalysts Unit : m^2/g

Sample	Fresh	HTA	SA	DeSOx
Pd/CeO_2	124	86	40	24
Pd/CeZr	126	60	38	47
Pd/CeZrPr	67	60	38	47

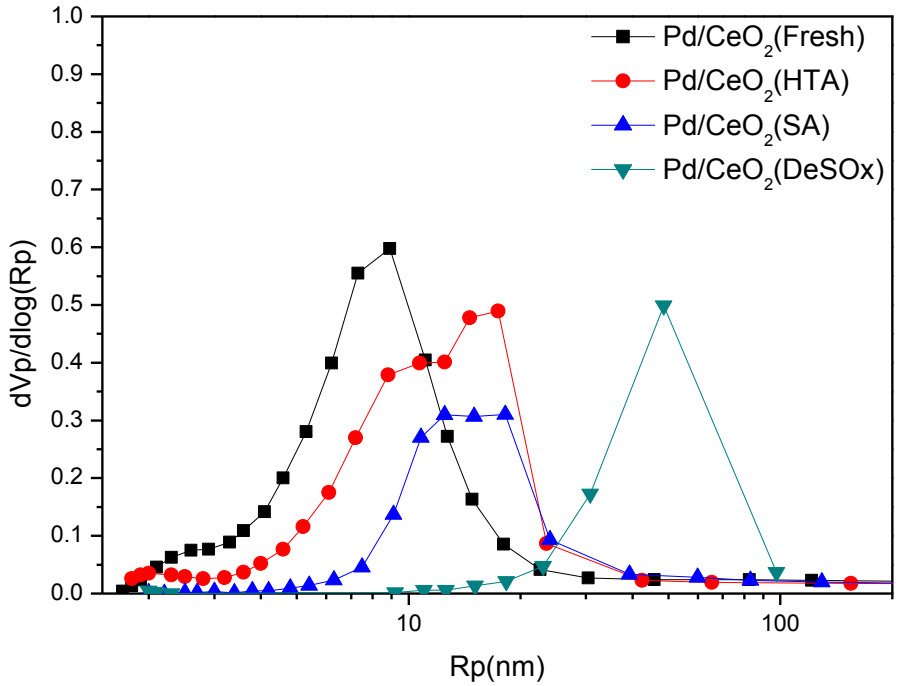

Fig. 5. Pore size distribution of Pd/CeO_2 catalysts (Fresh, HTA, SA, DeSOx).

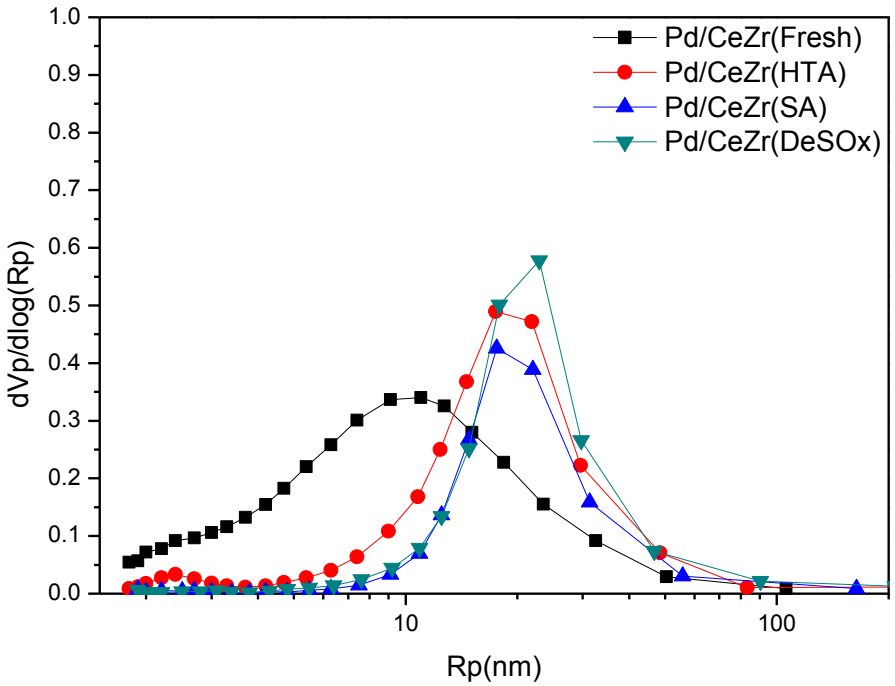

Fig. 6. Pore size distribution of Pd/CeZr catalysts (Fresh, HTA, SA, DeSOx).

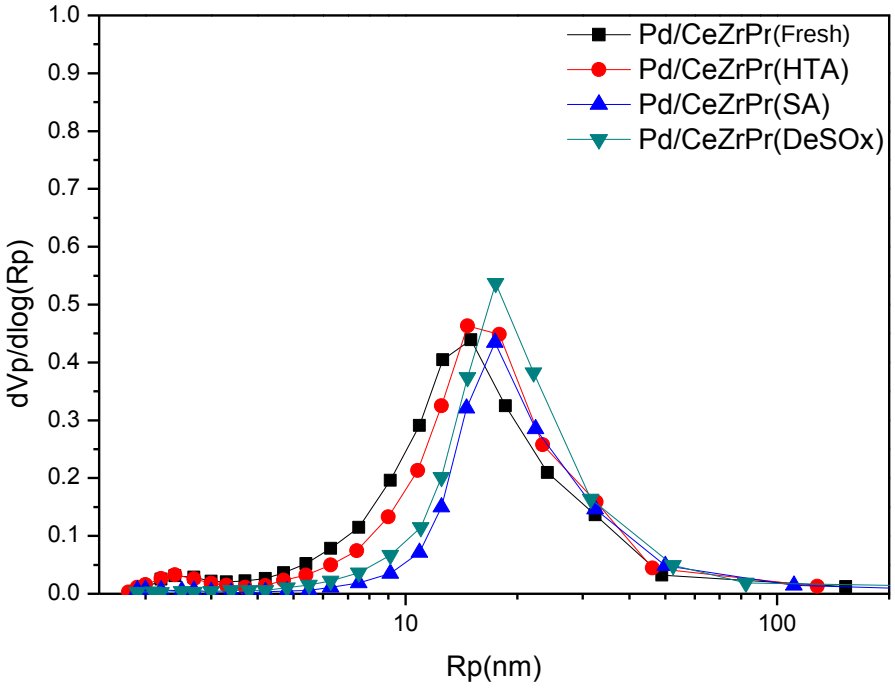

Fig. 7. Pore size distribution of Pd/CeZrPr catalysts (Fresh, HTA, SA, DeSOx).

3.3. CO-chemisorption

CO-chemisorption results of Pd catalysts are listed in Table 3. It has been researched that Pd dispersion and particle size are important factors for catalytic activities [49, 50]. In Table 3, it is shown that Pd is well dispersed and particle size is small. Especially CeO_2 catalyst has higher dispersion of Pd. Those results are in good agreement with the literature [38, 50]. However, after HTA process, the dispersion of Pd on CeO_2 is significantly reduced. The addition of Zr and Pr can stabilize Pd and maintain Pd particle size.

3.4. H_2-TPR

Fig. 8, 9 show H_2-TPR profiles of the Fresh and HTA catalysts. The reducibility of catalysts is an important feature affecting its catalytic ability and H_2-TPR is a common method to look into the reducibility of samples [51]. Three reduction peaks are observed, designated as peak α, β and γ, respectively. It is reported that PdO is reduced to Pd with H_2 gas at room temperature [51]. The strong low-temperature reduction peak α and β below 150 ℃ are mainly attributed to the reduction of PdO cluster and PdO at metal-support interface, respectively. The large intensity of β peak originates from oxygen back-spillover of the supprot [51-53]. The small peak in the range of 150-400 ℃, i.e. γ is the reduction of surface oxygen [51, 53, 54]. The negative peak of Pd/CeZr

samples in front of α peak is commonly attributed to the decomposition of PdH_x [52]. In the Fig. 8, the Fresh catalysts show lower intensity and broad temperature range of α and β peak, implying that there is a various particle size and weak interaction between PdO and support. The small particles are more readily to be reduced [51]. However, The peak α and β of the Pr added catalyst almost overlap each other, representing that Pr improves the oxygen mobility of the support. In the case of HTA catalysts (as shown in Fig. 9), in comparison with the Fresh samples, the intensity of peak α and β increases and the temperature shifts to lower region. This result indicates that the interaction between Pd and support is strengthened. It has positive effect on catalytic activity. The seperation of peak α and β of Pd/CeZrPr catalyst is due to addition of Pr, which stabilizes the PdO species [52, 53]. The surface reduction peak of catalysts, namely γ, decreases after HTA process because of sintering.

Table 3
The Pd dispersion and mean particle size by CO-chemisorption

Sample		Dispersion (%)	Mean particle size (nm)
Pd/CeO_2	Fresh	70.5	1.3
	HTA	57	2.0
Pd/CeZr	Fresh	41.2	2.1
	HTA	40.6	2.8
Pd/CeZrPr	Fresh	42.6	2.6
	HTA	44	2.6

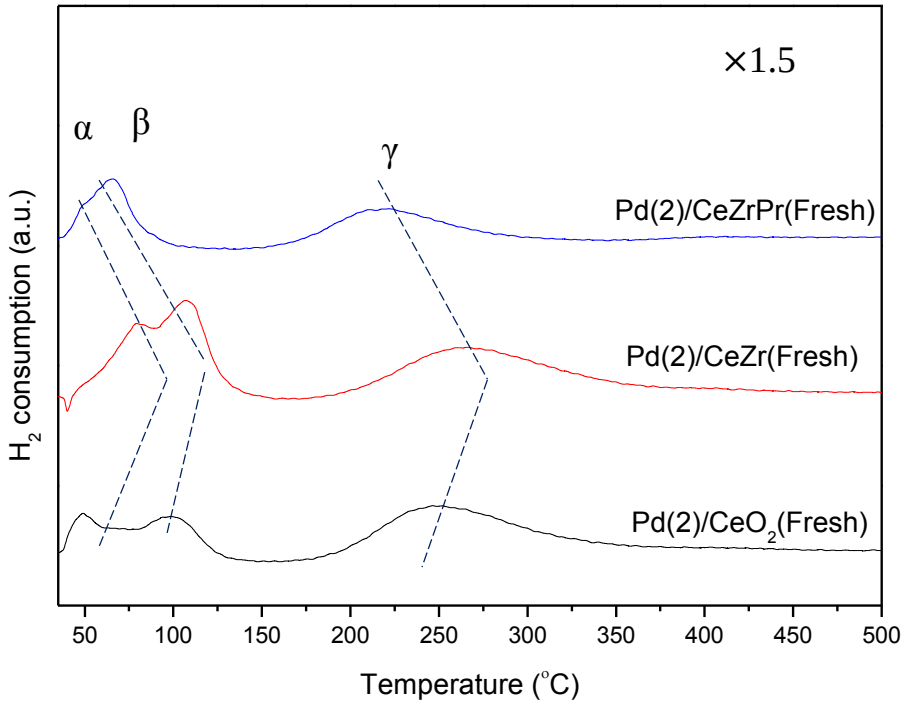

Fig. 8. H_2-TPR spectra of Fresh catalysts.

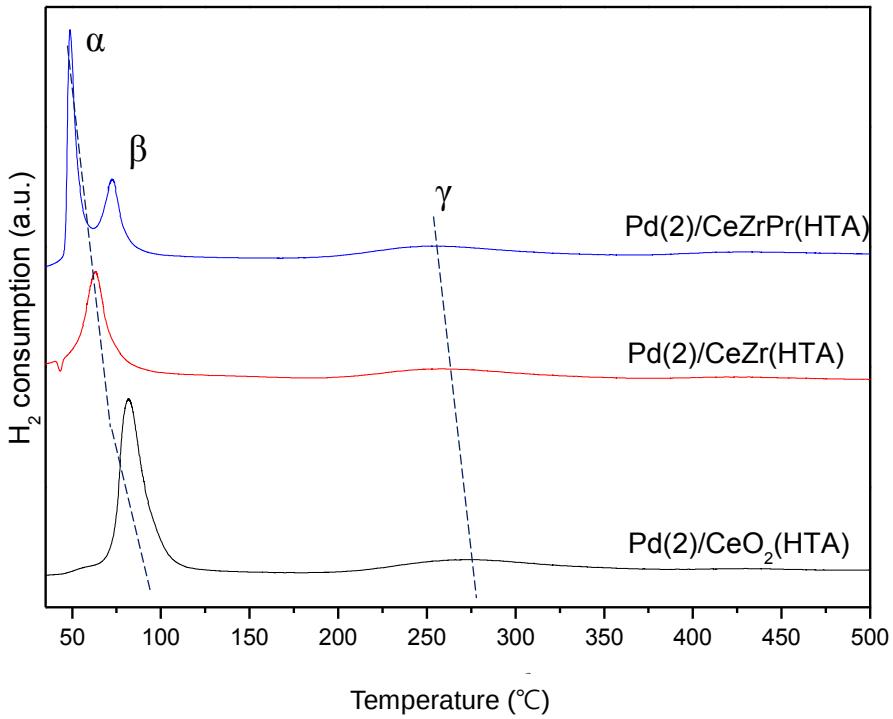

Fig. 9. H_2-TPR spectra of HTA catalysts.

3.5. FT-IR

FT-IR is performed to reveal sulfur amount and species. Fig. 10, 11 show IR spectra of SA and DeSOx samples. In the Fig. 10, The IR peaks of bulk sulfate species on SA samples present a broad band around 1145 cm^{-1} with shoulders at 1260 and 980 cm^{-1} [37, 40, 41, 55]. In addition, the intensity of the bulk sulfate peaks on the CeO_2 is much larger than mixed-oxide samples, indicating that pure CeO_2 more easily adsorbs sulfur. In fact, it is reported that the ZrO_2 only forms surface sulfate [40]. As can be seen in the Fig. 10, the intensity of the bulk sulfate peaks is dependent on the Ce content. However, Pd/CeZrPr sample exhibits slightly higher intensity than Pd/CeZr, though the Ce content of Pd/CeZrPr is smaller than Pd/CeZr. This result suggests that Pr also forms bulk sulfate. Therefore, the bulk sulfate is attributed to $Ce(SO_4)_2$ and $Pr_2(SO_4)_3$ [40]. After DeSOx process, the $Ce(SO_4)_2$ peaks decrease to zero. However, the IR peak of surface sulfate (at 1360 cm^{-1}) [40, 55] is not eliminated. Because of its thermal stability, surface sulfate is more difficult to remove [40, 55].

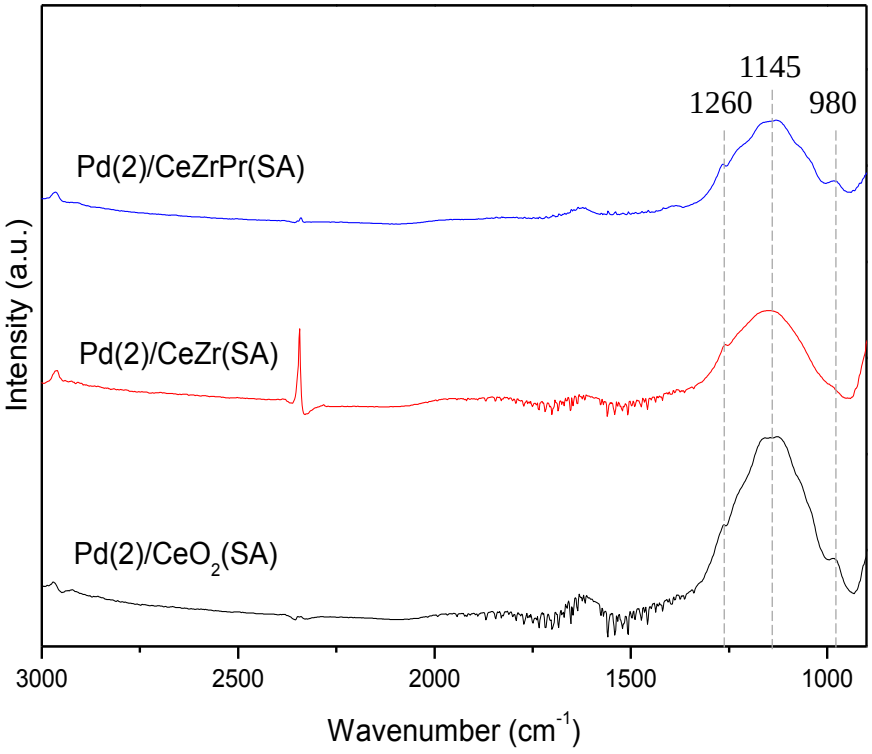

Fig. 10. FT-IR spectra of SA catalysts.

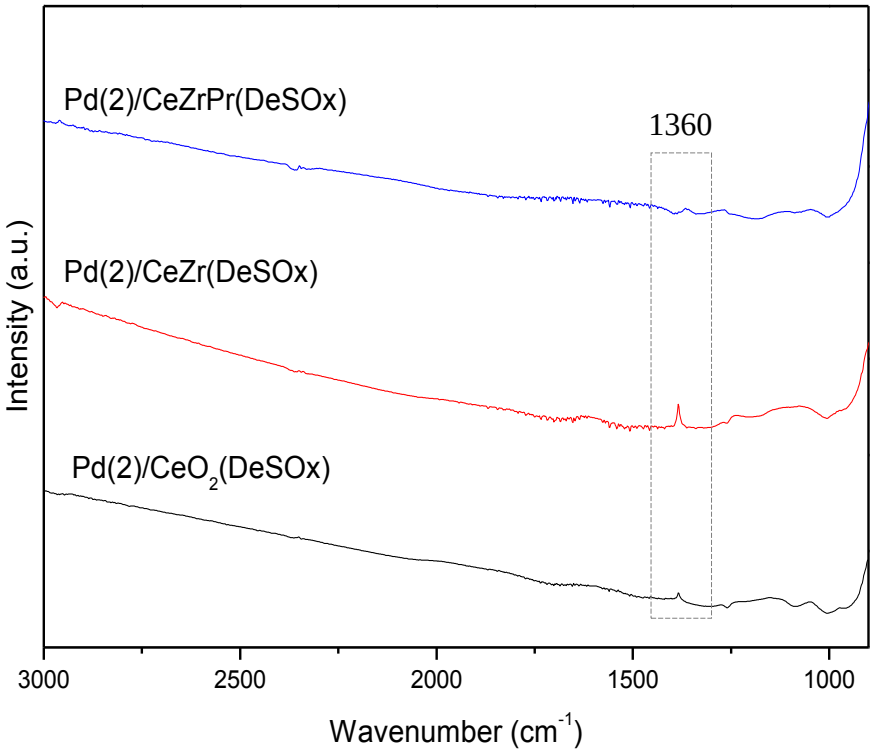

Fig. 11. FT-IR spectra of DeSOx catalysts.

3.6. SO_2-TPD

Fig. 12 shows SO_2 emission during the DeSOx treatment of sulfated samples. During the heating, most of sulfur species were decomposed as SO_2 with the peak at 710 ℃ and 750 ℃ for mixed-oxide and pure CeO_2 respectively. The amount of SO_2 desorbed from pure CeO_2 is much larger than that of mixed-oxide samples. Besides, Pr added sample has slightly higher intensity than Pd/CeZr, which is corresponding to the FTIR results described above. Moreover, it is worth noticing that the temperature of desorption from pure CeO_2 is higher than that of mixed-oxides, demonstrating that the sulfur species on mixed-oxide are more easily decomposed than pure CeO_2.

3.7. Elemental analysis

Elemental analysis results (as listed in Table 4) are additional evidence to support FTIR and SO_2-TPD results. The amount of sulfur in Pd/CeO_2, Pd/CeZr and Pd/CeZrPr is 4.7, 2.6 and 3wt%, respectively. After DeSOx treatment, the catalysts contain small amount of sulfur, which refers to surface sulfate identified in the FTIR section. While, the amount of sulfur adsorbed on catalysts is influenced by the Ce content, it displays nonlinear relationship. In other words, the ratio S to Ce of SA samples is different among samples. The catalysts containing Zr have smaller S/Ce ratio. Those results imply that Zr has an effect on inhibiting SO_2 adsorption on CeO_2 site.

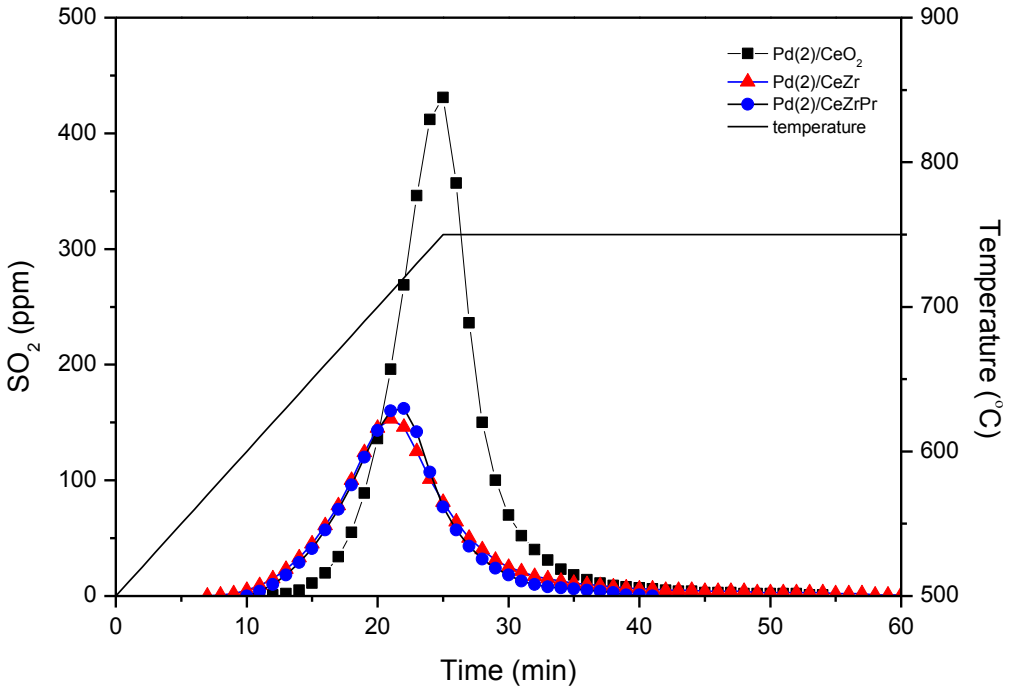

Fig. 12. SO_2-TPR peak of catalysts.

Table 4
The amount of sulfur in the catalysts by Elemental analysis

Sample	SA (wt%)	DeSOx (wt%)	S/Ce, (Ce+Pr) mole ratio of SA sample
Pd/CeO_2	4.7	0.6	0.27
Pd/CeZr	2.6	0.4	0.21
Pd/CeZrPr	3.0	0.5	0.26 (0.23)

3.8. CO oxidation activity

The CO oxidation results are shown in Fig. 13-15 with a series of various treatment. And T_{50} (The temperature of 50% conversion) is included in Table 5. In the Table 5, on the sample of Fresh, it appears that the catalytic activity of Pd/CeO_2 was higher than that of Pd/CeZr and Pd/CeZrPr. This is clearly due to high surface area and Pd dispersion (Table 2, 3). On the other hand, even though, the surface area of Pd/CeZrPr is less than a half of Pd/CeZr, the CO oxidation ability is similar. Pr with CeZr, causes an enhancement of its activity. When the catalyst samples were aged in hydrothermal condition for 25h, the reduction of the surface area is observed. Also, Pd dispersion of catalysts is reduced or remain unchanged. In spite of those results, an increase in the CO oxidation activity of all the samples is observed. The light-off temperatures shift about 13 ℃ to lower region. Therefore, this would be due to enhancement of Pd and support interaction described in the H_2-TPR section. In accordance with the results for Fresh sample described above, no strong relationship between CO oxidation and surface area of catalyst is observed. Pd dispersion, also, is not primary factor of CO oxidation. It can be suggested that the surface properties, such as Pd and support interaction have more profound effect on CO oxidation ability.

Pd on Ce-based support catalysts have alternative mechanism for CO oxidation, depending on temperature range [41, 56]. At low temperature region,

the reaction arises mostly between the adsorbed CO on Pd and the oxygen of surface CeO_2. When the reaction temperature increases, the surface reaction occurs between the adsorbed CO and O_2 [56].

During the sulfation, $Ce(SO_4)_2$ from Ce and SO_2, causes sintering, blocks the active site and decreases the surface area. In addition, on account of interruption of oxygen back-spillover from CeO_2 to Pd surface, Pd and support connection is weakened [41]. For this reason, the low temperature oxidation disappears. As can be seen in Fig. 13-15, all of SA samples exhibit steep and high light-off temperature. Since, especially, the Pr may help CO oxidation through its OSC ability, it partly redeems the deterioration of CO oxidation activity.

After regeneration process, sulfate on SA samples decomposes to SO_2 and O_2. Additionally, all of catalysts partially recover its low temperature activity. In case of Pd/CeO_2, sulfur adsorption and desorption lead to structural collapse, which causes sintering and reduction of surface area (Table 2, 3). Therefore, despite restoration of its low temperature activity, high temperature CO oxidation ability is worse than that of sulfated sample. Especially, the recovery of Pd/CeZr is remarkable result. This is due to its structure stability structure toward sulfur. From the results, it is found that Pd/CeZr has notable sulfur durability.

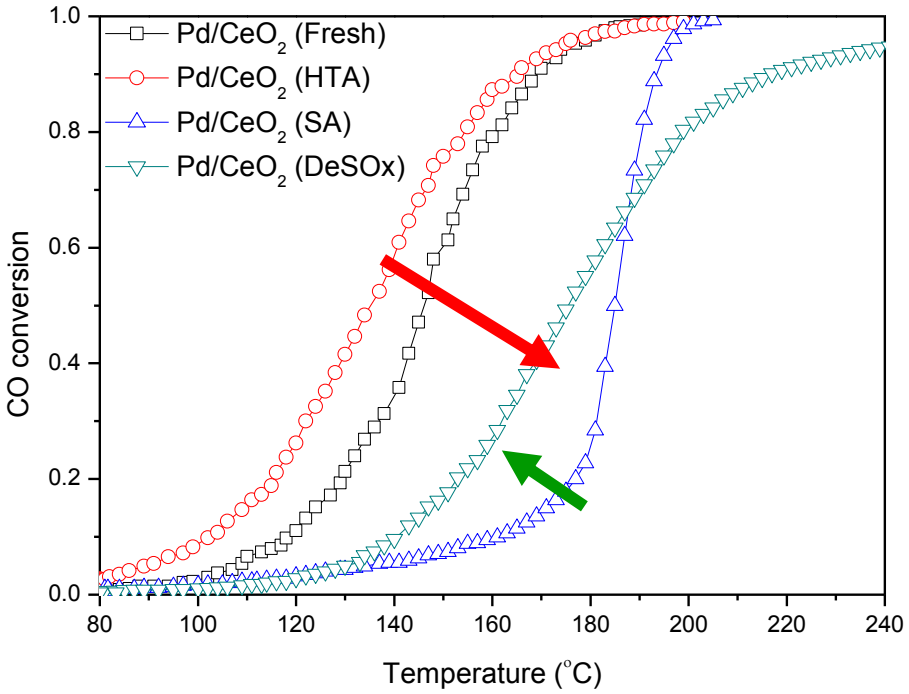

Fig. 13. CO conversion of Pd/CeO_2 catalysts (Fresh, HTA, SA, DeSOx).

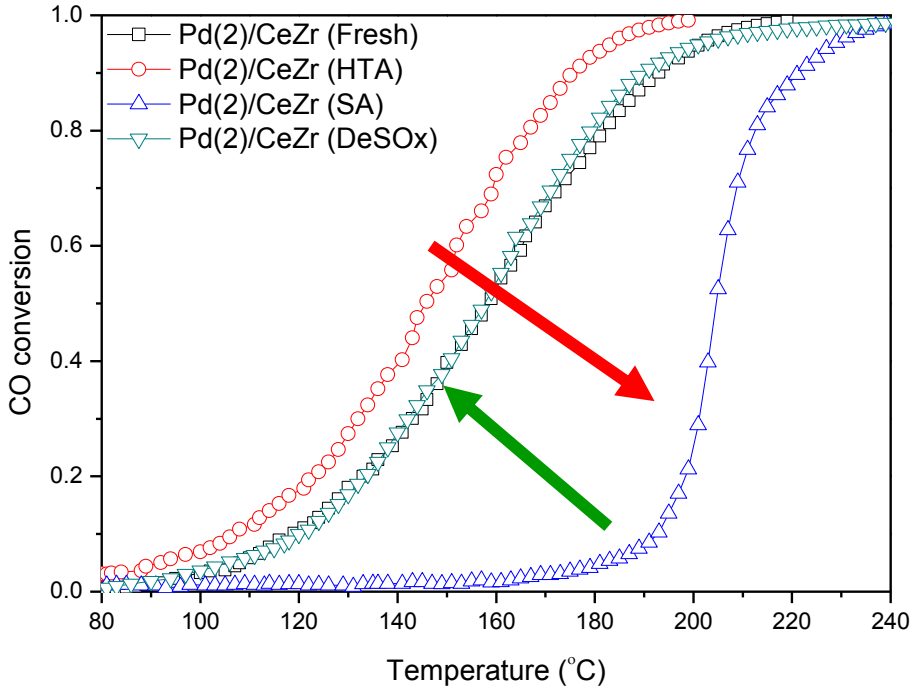

Fig. 14. CO conversion of Pd/CeZr catalysts (Fresh, HTA, SA, DeSOx).

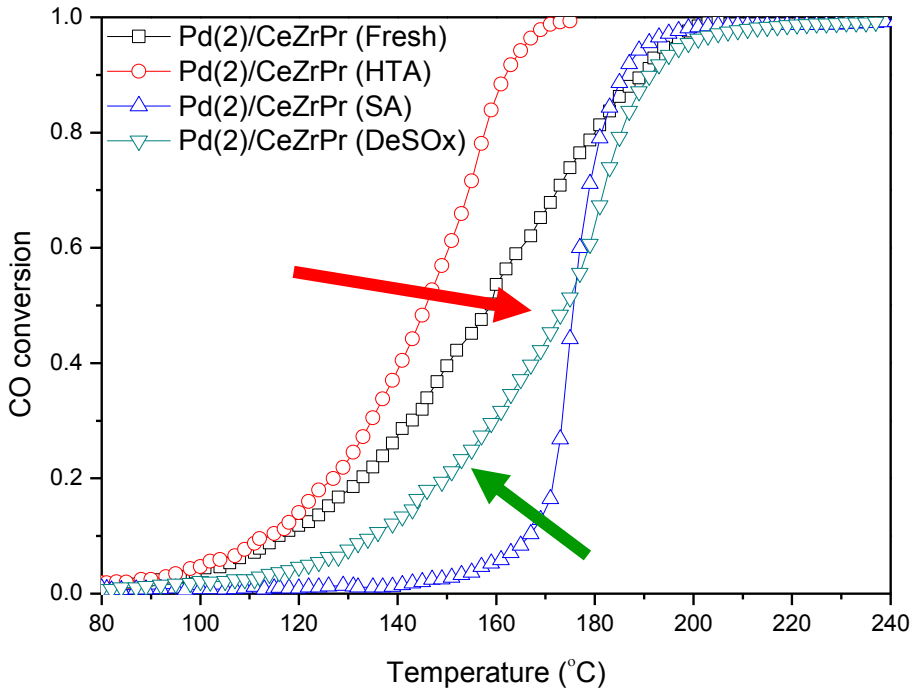

Fig. 15. CO conversion of Pd/CeZrPr catalysts (Fresh, HTA, SA, DeSOx).

Table 5
The T_{50} of CO oxidation

Unit : ºC

Sample	Fresh	HTA	SA	DeSOx
Pd/CeO_2	146	135	185	176
Pd/CeZr	159	146	204	156
Pd/CeZrPr	159	146	176	174

Chapter 4. Conclusion

In this work, to understand component effect for sulfur poisoning, various pretreatments and characteristics were carried out. At Fresh samples, Pd/CeO_2 has the highest CO oxidation reactivity due to its high surface area and Pd dispersion. The hydrothermal aging procedure improves Pd and support interaction, resulting in enhancement of catalytic ability. All of catalysts deactivate after sulfur aging. Among the SA samples, Pd/CeZrPr has superior catalytic activity, because Pr supplements the interaction between Pd and support through OSC property. After DeSOx process, even though $Ce(SO_4)_2$ formed during sulfation is removed, the catalytic activity of the catalysts only partially recovers. The interaction between Pd and support is destabilized by $Ce(SO_4)_2$ on sulfur aging samples. The DeSOx process of Pd/CeO_2 induces structural collapse of catalyst, which leads to decline in high temperature activity. The Pd/CeZr recovers almost its own initial activity after regeneration, indicating that the addition of Zr into Ce improves sulfur durability.

References

[1] P. G. Chen and J. M. Wang; Journal of Dynamic Systems Measurement and Control-Transactions of the Asme, *134*, (2012),

[2] S. R. Katare, J. E. Patterson and P. M. Laing; Industrial & Engineering Chemistry Research, *46*, (2007), *2445.*

[3] G. Corro; Reaction Kinetics and Catalysis Letters, *75*, (2002), *89.*

[4] L. Guzzella and A. Amstutz; Ieee Control Systems Magazine, *18*, (1998), *53.*

[5] M. Zheng, G. T. Reader and J. G. Hawley; Energy Conversion and Management, *45*, (2004), *883.*

[6] A. Russell and W. S. Epling; Catalysis Reviews-Science and Engineering, *53*, (2011), *337.*

[7] S. S. Gill, J. M. Herreros, A. Tsolakis, D. M. Turner, E. Miller and A. P. E. York; Rsc Advances, *2*, (2012), *10400.*

[8] F. J. P. Schott, S. Steigert, S. Zuercher, M. Endisch and S. Kureti; Chemical Engineering and Processing, *62*, (2012), *54.*

[9] J. Y. Chin, S. A. Batterman, W. F. Northrop, S. V. Bohac and D. N. Assanis; Energy & Fuels, *26*, (2012), *6737.*

[10] P. I. Jalava, P. Aakko-Saksa, T. Murtonen, M. S. Happo, A. Markkanen, P. Yli-Pirila, P. Hakulinen, R. Hillamo, J. Maki-Paakkanen, R. O. Salonen, J. Jokiniemi and M. R. Hirvonen; Particle and Fibre Toxicology, *9*, (2012),

[11] L. Lizarraga, S. Souentie, A. Boreave, C. George, B. D'Anna and P. Vernoux; Environmental Science & Technology, *45*, (2011), *10591.*

[12] P. Geng, C. D. Yao, L. J. Wei, J. H. Liu, Q. G. Wang, W. Pan and J. Y. Wang; Fuel, *123*, (2014), *1.*

[13] G. A. Westphal, J. Krahl, A. Munack, Y. Rusche, O. Schroder, E. Hallier,

T. Bruning and J. Bunger; Environmental Science & Technology, *46*, (2012), *6417.*

[14] M. R. Ward, T. Hyde, E. D. Boyes and P. L. Gai; Chemcatchem, *4*, (2012), *1622.*

[15] I. Lefort, J. M. Herreros and A. Tsolakis; Environmental Science & Technology, *48*, (2014), *2361.*

[16] L. Zhu, C. S. Cheung, W. G. Zhang, J. H. Fang and Z. Huang; Fuel, *113*, (2013), *690.*

[17] P. G. Chen and J. M. Wang; Journal of the Franklin Institute-Engineering and Applied Mathematics, *350*, (2013), *1992.*

[18] P. Rounce, A. Tsolakis and A. P. E. York; Fuel, *96*, (2012), *90.*

[19] Regulation (EC) NO 595/2009, <http://eur-lex.europa.eu/LexUriServ/LexUriServ.do?uri=OJ:L:2009:188:0001:0013:EN:PDF>

[20] Regulation (EC) NO 715/2007, <http://eur-lex.europa.eu/LexUriServ/LexUriServ.do?uri=OJ:L:2007:171:0001:0016:EN:PDF>

[21] D. Bounechada, G. Groppi, P. Forzatti, K. Kallinen and T. Kinnunen; Topics in Catalysis, *56*, (2013), *372.*

[22] Q. Y. Wang, B. Zhao, G. F. Li and R. X. Zhou; Environmental Science & Technology, *44*, (2010), *3870.*

[23] E. P. Brandt, Y. Y. Wang and J. W. Grizzle; Ieee Transactions on Control Systems Technology, *8*, (2000), *767.*

[24] R. M. Heck and R. J. Farrauto; Applied Catalysis a-General, *221*, (2001), *443.*

[25] D. K. Zhang, Y. Ma and M. M. Zhu; Proceedings of the Combustion Institute, *34*, (2013), *1869.*

[26] P. G. Chen and J. M. Wang; Control Engineering Practice, *22*, (2014), *81.*

[27] S. F. Ye, Y. H. Yap, S. T. Kolaczkowski, K. Robinson and D. Lukyanov;

Chemical Engineering Research & Design, *90*, (2012), *834.*

[28] S. Kolaczkowski, S. Ye, Y. Yap, K. Robinson and D. Lukyanov; Catalysis Today, *188*, (2012), *53.*

[29] J. Kim, C. Kim and S. J. Choung; Catalysis Today, *185*, (2012), *296.*

[30] S. Raux, A. Frobert and E. Jeudy; Topics in Catalysis, *52*, (2009), *1903.*

[31] M. V. Twigg; Catalysis Today, *117*, (2006), *407.*

[32] A. Morlang, U. Neuhausen, K. V. Klementiev, F. W. Schutze, G. Miehe, H. Fuess and E. S. Lox; Applied Catalysis B-Environmental, *60*, (2005), *191.*

[33] M. Kaneeda, H. Iizuka, T. Hiratsuka, N. Shinotsuka and M. Arai; Applied Catalysis B-Environmental, *90*, (2009), *564.*

[34] P. Gelin, L. Urfels, M. Primet and E. Tena; Catalysis Today, *83*, (2003), *45.*

[35] M. Chen and L. D. Schmidt; Journal of Catalysis, *56*, (1979), *198.*

[36] A. M. Venezia, L. F. Liotta, G. Pantaleo, V. La Parola, G. Deganello, A. Beck, Z. Koppany, K. Frey, D. Horvath and L. Guczi; Applied Catalysis a-General, *251*, (2003), *359.*

[37] P. Bazin, O. Saur, F. C. Meunier, M. Daturi, J. C. Lavalley, A. M. Le Govic, V. Harle and G. Blanchard; Applied Catalysis B-Environmental, *90*, (2009), *368.*

[38] M. Fernandez-Garcia, A. Martinez-Arias, A. Iglesias-Juez, A. B. Hungria, J. A. Anderson, J. C. Conesa and J. Soria; Applied Catalysis B-Environmental, *31*, (2001), *39.*

[39] L. F. Nascimento, R. F. Martins, R. F. Silva, P. C. de Sousa and O. A. Serra; Reaction Kinetics Mechanisms and Catalysis, *111*, (2014), *149.*

[40] T. Luo and R. J. Gorte; Applied Catalysis B-Environmental, *53*, (2004), *77.*

[41] H. M. Yang, G. X. Wei, X. Q. Wang, F. Lin, J. Wang and M. Q. Shen; Catalysis Communications, *36*, (2013), *5.*

[42] Y. Guo, G. Z. Lu, Z. G. Zhang, S. H. Zhang, Y. Qi and Y. Liu; Catalysis Today, *126*, (2007), *296.*

[43] C. Wen, Y. Liu, Y. Guo, Y. Q. Wang and G. Z. Lu; Surface Review and Letters, *20*, (2013),

[44] S. S. Deshmukh, M. H. Zhang, V. I. Kovalchuk and J. L. d'Itri; Applied Catalysis B-Environmental, *45*, (2003), *135.*

[45] P. Sudarsanam, B. Mallesham, P. S. Reddy, D. Grossmann, W. Grunert and B. M. Reddy; Applied Catalysis B-Environmental, *144*, (2014), *900.*

[46] I. Atribak, B. Azambre, A. B. Lopez and A. Garcia-Garcia; Applied Catalysis B-Environmental, *92*, (2009), *126.*

[47] D. Terribile, A. Trovarelli, J. Llorca, C. de Leitenburg and G. Dolcetti; Catalysis Today, *43*, (1998), *79.*

[48] R. Craciun, W. Daniell and H. Knozinger; Applied Catalysis a-General, *230*, (2002), *153.*

[49] A. Satsuma, K. Osaki, M. Yanagihara, J. Ohyama and K. Shimizu; Applied Catalysis B-Environmental, *132*, (2013), *511.*

[50] B. Wang, D. A. Weng, X. D. Wu and R. Ran; Applied Surface Science, *257*, (2011), *3878.*

[51] Q. Y. Wang, G. F. Li, B. Zhao, M. Q. Shen and R. X. Zhou; Applied Catalysis B-Environmental, *101*, (2010), *150.*

[52] R. Ran, H. W. Zhang, X. D. Wu, J. Fan and D. Weng; Journal of Rare Earths, *32*, (2014), *108.*

[53] Q. Y. Wang, G. F. Li, B. Zhao and R. X. Zhou; Journal of Molecular Catalysis a-Chemical, *339*, (2011), *52.*

[54] P. S. Lambrou and A. M. Efstathiou; Journal of Catalysis, *240*, (2006), *182.*

[55] M. Waqif, P. Bazin, O. Saur, J. C. Lavalley, G. Blanchard and O. Touret;

Applied Catalysis B-Environmental, *11*, (1997), *193*.

[56] H. Q. Zhu, Z. F. Qin, W. J. Shan, W. J. Shen and J. G. Wang; Journal of Catalysis, *233*, (2005), *41*.

요약(국문초록)

우수한 연료 경제성에서 오는 경제적 이득 때문에 디젤엔진은 많은 관심을 받고 있다. 하지만 디젤 엔진 배기 가스에 대한 규제가 점점 더 심해짐에 따라서 CO, hydrocarbons(HCs), soot 그리고 NOx 같은 유해한 가스들을 효과적으로 제거하기 위한 다양한 촉매 처리 시스템이 연구되고 있다. 디젤 산화 촉매 (DOC)는 CO와 연소 되지 않은 HCs을 CO_2와 H_2O로 산화시키는데 중요한 역할을 하는데 DOC가 제 기능을 적절하게 발휘하기 위해서는 낮은 산화 온도, 수열적 안정성 그리고 내황성이 중요하다. CeO_2는 oxygen storage capacity (OSC) 능력을 갖고 있어 DOC가 낮은 온도의 light-off curve를 얻는데 중요한 역할을 하는 지지체 물질이다. 하지만 CeO_2는 높은 온도와 황피독에 쉽게 활성을 잃는 성질이 있다. 이번 연구에서는 이런 단점들을 극복하기 위해 CeO_2와 비교하여 CeZr와 CeZrPr mixed-oxide solid solution을 지지체로 사용하였다.

촉매는 다양한 처리과정을 통해 제조 하였는데 우선 Pd 2wt%를 함침법으로 지지체에 담지한 후, 500 ℃에서 소성한 다음 750 ℃에서 수열처리 하였다. 2가지 방법으로 처리한 촉매들을 각각 “Fresh”, “HTA”라 표기하였다. 황피독 과정에서 HTA 촉매를

SO_2가스로 처리한 후, 이어서 재생과정을 진행하였다. 황피독 촉매와 재생촉매를 각각 “SA”, “DeSOx”라 나타내었다.

촉매에 물리화학적 특성 정보를 얻기 위해서 XRD, BET, FT-IR, Elemental analysis, CO-chemisorption, H_2-TPR 그리고 SO_2-TPD 분석을 진행하고 또한 다양한 전처리 촉매에 대해서 CO 산화 실험을 진행하였다.

Fresh 촉매들 중 높은 분산도와 표면적으로 인해 Pd/CeO_2가 가장 높은 CO 산화 활성을 보였다. 수열처리 이후 H_2-TPR 결과로부터 Pd과 지지체 사이의 상호작용이 강화 된다는 것을 확인 할 수 있었고 그 결과 모든 HTA촉매에 반응성이 증가하였다. 황 피독으로 인해 Pd/CeO_2에 $Ce(SO_4)_2$가 형성됨을 FT-IR실험을 통해 확인하였다. 황 피독 과정에서 형성된 $Ce(SO_4)_2$는 Pd 활성점을 막고 표면적을 감소 시킬 뿐만 아니라 CeO_2에서 Pd로의 oxygen back-spillover를 방해하여 Pd와 CeO_2 사이의 상호 작용을 약화시킨다. 그 결과 낮은 온도 영역에서의 촉매 활성이 감소 하였다. 황 피독 촉매중에 Pd/CeZrPr이 가장 우수한 촉매 활성을 보이는데 이는 Pr이 가지고 있는 OSC능력이 Pd과 지지체 사이에 상호작용을 도와 주기 때문이다. XRD와 BET결과를 통해 Pd/CeZr촉매가 뛰어난 내황성이 있음을

확인 할 수 있었고 촉매 재생 후에 반응 실험 결과 역시 Pd/CeZr이 가장 높은 반응성 회복 능력을 보여 우수한 내황성이 있음을 나타내었다. Pd/CeO_2의 경우 황 흡탈착으로 인해 구조적 붕괴가 일어나는데 이는 촉매의 소결을 일으키고 표면적을 감소시킨다. 따라서 Pd/CeO_2의 활성은 오히려 촉매를 재생하기 전보다 더 감소하였다.

본 연구에서는 황 흡탈착 과정중에 Pd/CeO_2촉매에 대하여 Zr과 Pr의 역할에 대해 확인하였다. Pr은 황 피독 도중 촉매 활성감소를 최소화 한다. CeO_2에 Zr 첨가는 황 흡탈착 과정 동안 황피독을 방해하고 구조특성을 유지시켜주며 탈황을 도와준다. 따라서 촉매 재생 후 높은 활성을 보인다.

주요어 : CO 산화, palladium 촉매, 세륨 옥사이드, 지르코늄, 프라세오디뮴, 황피독, 재생 촉매

학 번 : 2012-23269